

# ON THE ENHANCED INTERSTELLAR SCATTERING TOWARD B1849+005

T. JOSEPH W. LAZIO

Code 7213, Naval Research Laboratory, Washington, DC 20735-5351; joseph.lazio@nrl.navy.mil

Received 2003 May 8; accepted 2004 June 7

## ABSTRACT

This paper reports new Very Large Array (VLA) and Very Long Baseline Array (VLBA) observations of the extragalactic source B1849+005 (Galactic coordinates  $\ell = 33^\circ 44'$ ,  $b = +0^\circ 21'$ ) at frequencies between 0.33 and 15 GHz and the reanalysis of archival VLA observations at 0.33, 1.5, and 4.9 GHz. The structure of this source is complex, confirming previous suggestions, but interstellar scattering dominates the structure of the central component at least to 15 GHz. An analysis of the phase structure functions of the interferometric visibilities shows the density fluctuations along this line of sight to be anisotropic (axial ratio = 1.3) with a frequency-independent position angle and having an inner scale of roughly a few hundred kilometers. The anisotropies occur on length scales of order  $10^{15}$  cm ( $D/5$  kpc), which within the context of certain magnetohydrodynamic turbulence theories indicates the length scale on which the kinetic and magnetic energy densities are comparable. A conservative upper limit on the velocity of the scattering material is  $1800 \text{ km s}^{-1}$ , based on the lack of changes in the shapes of the 0.33 GHz images. In the 0.33 GHz field of view, there are a number of other sources that might also be heavily scattered, which would suggest that there are large changes in the scattering strength on lines of sight separated by a degree or less. Both B1849+005 and PSR B1849+00 are highly scattered, and they are separated by only  $13'$ . If the lines of sight are affected by the same “clump” of scattering material, it must be at least 2.3 kpc distant. However, a detailed attempt to account for the scattering observables toward these sources (angular broadening of the extragalactic source, pulse broadening of the pulsar, and upper limits on the angular broadening of the pulsar) does not produce a self-consistent set of parameters for a clump that can reproduce all three measured scattering observables. A clump of  $H\alpha$  emission, possibly associated with the  $H \text{ II}$  region G33.418–0.004, lies between these two lines of sight, but it seems unable to account for all of the required excess scattering.

*Subject headings:* galaxies: individual (B1849+005) — ISM: structure — pulsars: individual (B1849+00) — radio continuum: general — scattering

## 1. INTRODUCTION

Density fluctuations on subparsec scales in the interstellar plasma produce refractive index fluctuations. In turn, these refractive index fluctuations scatter radio radiation propagating through the plasma. The result is a rich set of observables including angular broadening of compact sources, pulsar intensity scintillations, and low-frequency variability of extragalactic sources (for reviews see Rickett 1990; Narayan 1992).

The density fluctuations responsible for interstellar scattering appear to be well parameterized by a power-law power spectrum. In many cases the spectral index of the power spectrum is near  $11/3$ , the value predicted by the Kolmogorov theory of turbulence for neutral, incompressible unmagnetized fluids. As the interstellar plasma is compressible, ionized, and magnetized, it would appear to violate these assumptions. There has been recent progress in understanding how a Kolmogorov-like spectrum could arise in a magnetized plasma, however (Lithwick & Goldreich 2003 and references within). Combined with the large Reynolds number of the interstellar plasma, this suggests that the density fluctuations arise from a turbulent process. A small number of lines of sight toward pulsars are notable counterexamples, having spectral indices larger than 4 (Hewish et al. 1985; Woloszcan & Cordes 1987; Gupta et al. 1988; Clegg et al. 1993) or an index approaching 4 (Spangler & Gwinn 1990; Moran et al. 1990; Wilkinson et al. 1994; Molnar et al. 1995). An index larger than 4 arises from a random distribution of density fluctuations, while an index approaching 4 is interpreted as a modification of the power-law spectrum by an inner scale indicative of a dissipative scale for

the turbulence. Thus, determination of the spectral index of the density fluctuation spectrum can provide clues about the mechanisms by which the density fluctuations originate.

Wilkinson et al. (1994) showed that not only can a density spectral index be obtained, but multifrequency observations may probe the organization and orientation of the density fluctuations responsible for scattering. They showed that the axial ratio and position angle of Cyg X-3 are frequency dependent, a frequency dependence that they interpreted in terms of an increasingly ordered magnetic field on smaller and smaller scales. Trotter et al. (1998) showed subsequently that the axial ratio and orientation of the scattering disk of NGC 6334B also exhibited a frequency dependence. Thus, scattering observations may be a probe of the magnetic field on subparsec scales.

Conversely, OH masers seen toward the Galactic center exhibit some of the most extreme anisotropic images seen anywhere in the Galaxy (van Langevelde et al. 1992; Frail et al. 1994). While it is not possible to measure a frequency dependence for the scattering disks of the OH masers, the scattering disk of Sgr A\* exhibits no change in its axial ratio or orientation over nearly 1.5 decades in frequency (Lo et al. 1985; Jauncey et al. 1989; Alberdi et al. 1993; Yusef-Zadeh et al. 1994; Marcaide et al. 1999; Reid et al. 1999). It is not yet clear what the different frequency behavior for the scattering diameters of Cyg X-3 and NGC 6334B versus Sgr A\* represents. Possibilities might include a difference between the scattering media in the Galactic center and disk or a much stronger magnetic field in the Galactic center.

The source B1849+005 (Galactic coordinates  $\ell = 33^\circ 44'$ ,  $b = +0^\circ 21'$ ) is seen along the third-most highly scattered line of

TABLE 1  
OBSERVING LOG

Frequency (GHz)	Epoch	Array	Bandwidth (MHz)	Recorded Polarization	On-Source Time (hr)	rms Image Noise (mJy beam <sup>-1</sup> )
0.33.....	1987 Aug 20	VLA (A-conf.)	3.0	R	0.28	80
0.33.....	1998 Mar 19	VLA (A-conf.)	3.0	R, L	4.9	4.4
1.5.....	1987 Aug 20	VLA (A-conf.)	43.75	R	0.375	0.32
2.3.....	2002 Aug 23	VLBA (FD, KP, OV, LA, PT)	32	R, L	1.2	...
4.9.....	1987 Aug 20	VLA (A-conf.)	50	R	0.017	1
5.0.....	1998 Mar 29	VLBA+VLA1	56	L	1.4	0.39
8.4.....	1998 Mar 29	VLBA+VLA1	64	R	0.89	0.51
15.....	1998 Mar 29	VLBA+VLA1	64	L	1.4	0.84
22.....	1998 Mar 29	VLBA+VLA1	64	L	1.4	...

sight known, after the Galactic center (Lazio & Cordes 1998) and NGC 6334B (Trotter et al. 1998). Spangler et al. (1986) conclude that it is extragalactic because it is a compact, flat-spectrum variable source. Further evidence that B1849+005 is extragalactic is found by comparing its H I absorption spectrum to that of the pulsar PSR B1849+00, which is 13' from B1849+005. It must be more distant than PSR B1849+00 and is probably at least 25 kpc distant (van Gorkom et al. 1982; Dickey et al. 1983; Clifton et al. 1988; Frail & Weisberg 1990). PSR B1849+00 is also the most heavily scattered pulsar known, with a pulse broadening time of 0.2 seconds at 1.4 GHz. Thus, a comparison of the lines of sight to B1849+005 and PSR B1849+00 can probe changes in the scattering medium transverse to the line of sight on scales not normally accessible.

This paper reports multifrequency observations of B1849+005, spanning nearly two decades in frequency, that are used to reassess the structure and nature of B1849+005 and constrain the scattering properties along this line of sight. In § 2 I describe the observations and data reduction, in § 3 I use these observations to extract various scattering parameters along the line of sight to B1849+005, in § 4 I combine my observations with those from the literature to probe the scattering environment around B1849+005 and particularly toward PSR B1849+00, and in § 5 I summarize my results.

## 2. OBSERVATIONS AND ANALYSIS

The scattering disk of B1849+005 is large enough that it can be resolved by a range of frequencies and baselines accessible with the Very Large Array (VLA) and Very Long Baseline Array (VLBA). The details of the observations and data reduction for the VLA and VLBA observations are sufficiently different that I discuss them separately. Table 1 presents the observing log.

### 2.1. VLA Observations (0.33–4.9 GHz)

#### 2.1.1. 0.33 GHz

Observations were obtained at 0.33 GHz with the A-configuration of the VLA on 1998 March 19. The sources 3C 48 and 3C 286 were used in calibrating the visibility amplitudes, and the VLA calibrator J1859+1259 was used in calibrating the visibility phases. Standard calibration and radio frequency interference (RFI) excision procedures were used within the NRAO Astronomical Image Processing System (AIPS). Several iterations of self-calibration and imaging were used to approach the thermal noise level. During imaging, a polyhedron algorithm (Cornwell & Perley 1992) was used to account for the noncoplanar nature of the VLA.

At 0.33 GHz the field of view is large (2.5 FWHM) and contains many sources. In order to isolate the visibilities from B1849+005, the following procedure was used. Sources within the primary beam field of view as well as strong sources outside the primary beam were identified in the NRAO VLA Sky Survey (Condon et al. 1998). Seventy-three such sources were identified, including B1849+005. Following Perley (1989), the Fourier transform of all of the sources was subtracted from the visibility data, a modest amount of additional data editing was performed, and the Fourier transform of only B1849+005 was added back to the visibility data.

The imaging was done with the visibility data at the spectral resolution at which it was acquired (97.7 kHz channels), both to avoid bandwidth smearing and to make RFI easier to identify. After removing all other sources, bandwidth smearing is no longer an issue, and the data were averaged over frequency. Also, in order to reduce the data volume before further processing, the visibilities were averaged from 10 to 240 s. This time and frequency averaging also further “dilutes” the impact of any unsubtracted sources or errors in the models of the sources that were subtracted.

I also obtained from the VLA Archive (program AS305) A-configuration VLA observations of B1849+005 acquired originally on 1987 August 20 by Fey et al. (1991). The calibration of these observations was similar (but with the VLA calibrator B1938–155 used to calibrate the phases), but given the relatively limited amount of visibility data (15 minute observation), only B1849+005 was imaged, rather than using targeted facetting. The limited visibility data also implies a higher noise level and limited image fidelity. Figure 1 shows the resulting 0.33 GHz images of B1849+005.

#### 2.1.2. 1.5 GHz

The nominal resolution of the A-configuration of the VLA at 1.5 GHz is approximately 1".5. The expected scattering diameter of B1849+005 at this frequency is approximately 0".3. “Superresolution” imaging can provide better than the nominal resolution by appropriate weighting of the visibility data at the cost of a modest reduction in sensitivity (Briggs et al. 1999). Given the strength of this source (~0.5 Jy at 1.5 GHz), this is an acceptable trade-off.

I obtained from the VLA Archive (program AS305) A-configuration VLA observations of B1849+005 acquired originally on 1987 August 20 by Fey et al. (1991) with the aim of imaging the source at superresolution. The source 3C 286 was used to calibrate the visibility amplitude, and the VLA calibrator B1821+107 was used in calibrating the visibility phases. Standard calibration procedures were used, including a number of iterations of phase self-calibration.

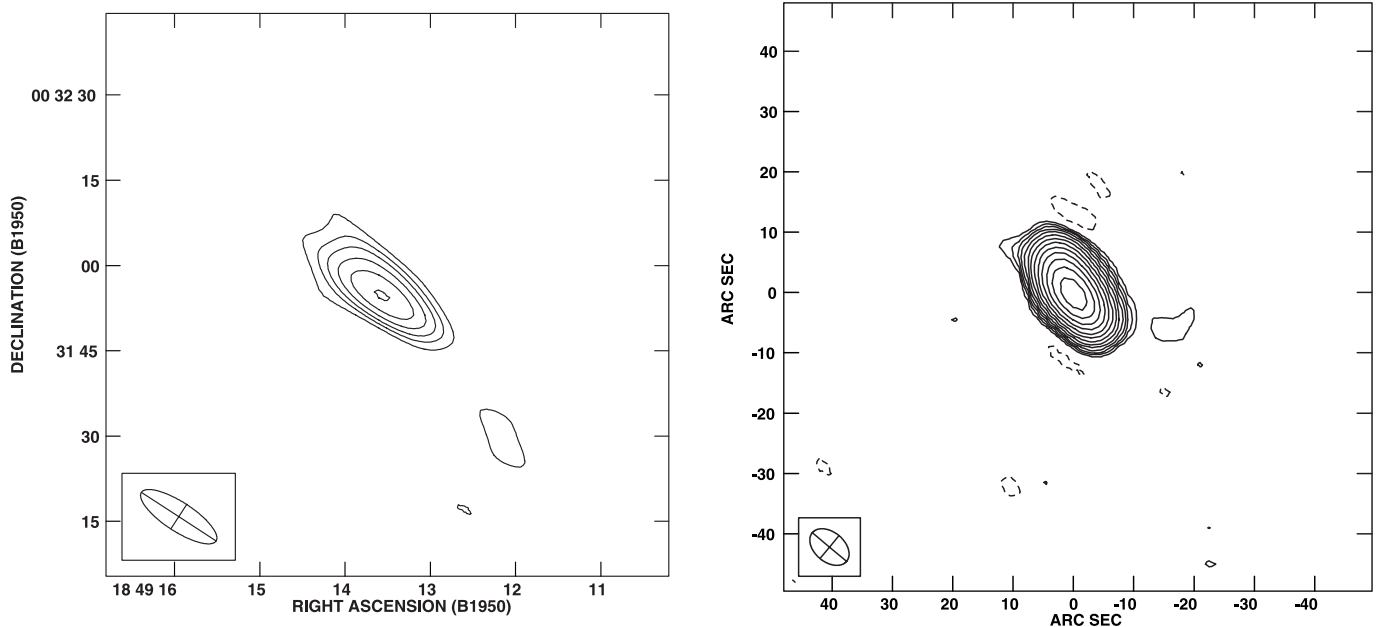


FIG. 1.—B1849+005 at 0.33 GHz. *Left*: The image resulting from the 1987 August 20 observations. The rms noise level is  $80 \text{ mJy beam}^{-1}$ , and the contour levels are  $80 \text{ mJy beam}^{-1} \times -3, 3, 5, 7.07, 10, \dots$ . The beam is  $15''.7 \times 5''.1$  and is shown in the lower left. *Right*: The image resulting from the 1998 March 19 observations. The rms noise level is  $4.4 \text{ mJy beam}^{-1}$ , and contour levels are  $4.4 \text{ mJy beam}^{-1} \times -3, 3, 5, 7.07, 10, \dots$ . The beam is  $7''.4 \times 4''.9$  and is shown in the lower left.

As was done in imaging the 0.33 GHz observations, a polyhedral algorithm was used to account for the non-coplanarity of the VLA and image the entire field of view ( $30'$  FWHM). In practice, the number of other sources in the field was sufficiently small and their flux densities sufficiently low that ignoring the VLA's noncoplanarity would have made little difference in the final image.

Experiments with the amount of superresolution used showed that reasonable choices for the amount of weighting led to resolution improvements by as much as 20% (i.e., decrease in beam diameter). Figure 2 shows the resulting image of B1849+005 with a modest amount of superresolution (10% reduction in the beam diameter). In practice, the amount of superresolution used made little difference in the measured image diameter, but the measured image diameter is smaller than the beam diameter. Decreasing the beam diameter increases the ratio of the image diameter to the beam diameter and therefore increases the robustness of the measured image diameter, particularly if the image diameter is smaller than the beam diameter, as is the case here.

### 2.1.3. 4.9 GHz

Fey et al. (1991) also obtained a single hour angle (1 minute duration) on B1849+005 at 4.9 GHz during the same set of observations used to acquire the 1.5 GHz observations. Based on the results of imaging the 1.5 GHz observations, these 4.9 GHz observations were reanalyzed also. The source 3C 286 was used to calibrate the visibility amplitude, and the VLA calibrator B1821+107 was used in calibrating the visibility phases. Standard calibration procedures were used, including a small number of iterations of phase self-calibration. Figure 3 shows the resulting image.

## 2.2. VLBA Observations (2.3–22 GHz)

Observations at 5, 8.4, 15, and 22 GHz were obtained with the VLBA and one antenna of the VLA on 1998 March 29. Observations at 2.3 GHz were obtained with only the inner antennas of the VLBA on 2002 August 23. No fringes were

detected at 22 GHz. The lack of a detection at 22 GHz is consistent with the lower sensitivity of the VLBA at this frequency relative to the other frequencies observed. At the other frequencies, the correlated visibilities were fringe fit and amplitude calibrated in the standard fashion within AIPS. Fringe-fitting intervals were 2.5–3 minutes. The calibrated visibilities were then exported to the Caltech Difmap program for hybrid mapping.

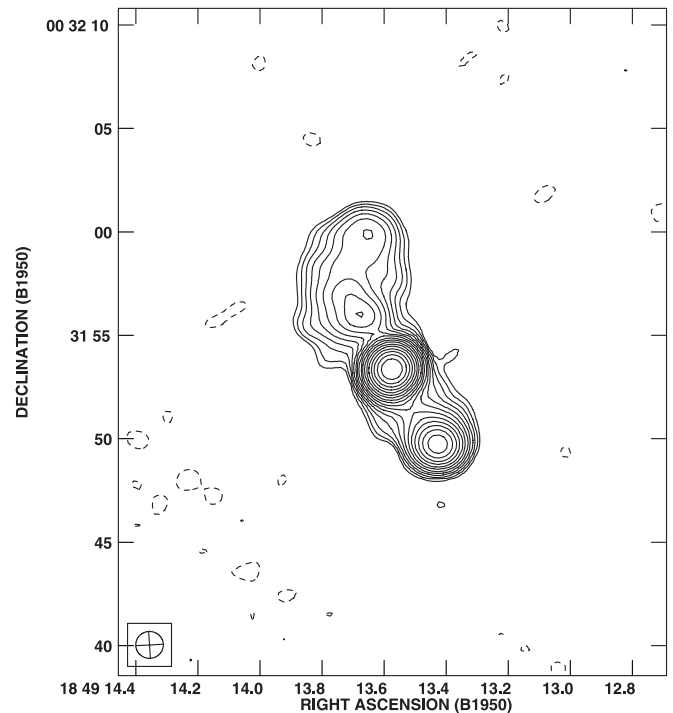


FIG. 2.—B1849+005 at 1.5 GHz, imaged using a modest amount of super-resolution to obtain a 10% reduction in the nominal beam diameter. The rms noise level is  $0.32 \text{ mJy beam}^{-1}$ , and contour levels are  $0.32 \text{ mJy beam}^{-1} \times -3, 5, 7.07, 10, 14.1, 20, \dots$ . The beam is  $1''.3 \times 1''.3$  and is shown in the lower left.

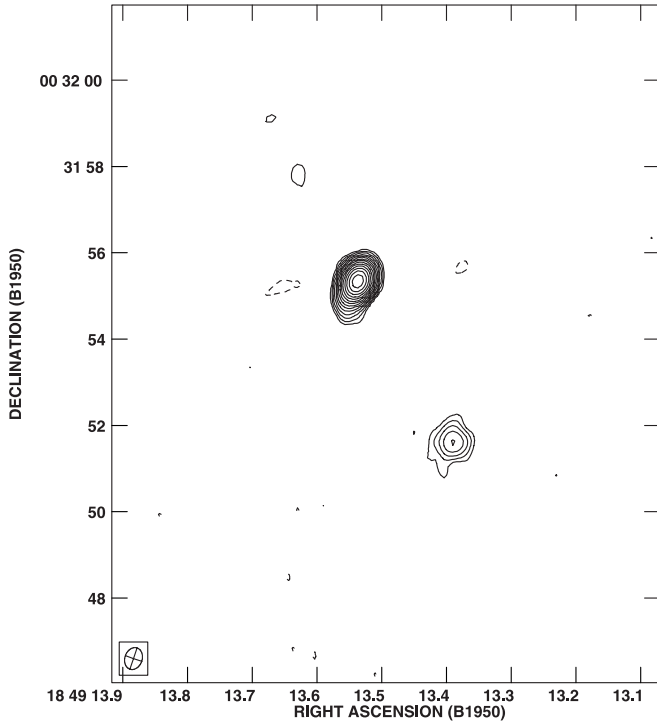


FIG. 3.—B1849+005 at 4.9 GHz, as observed by the VLA. The rms noise level is  $1 \text{ mJy beam}^{-1}$ , and contour levels are  $1 \text{ mJy beam}^{-1} \times -3, 5, 7.07, 10, 14.1, \dots$ . The beam is  $0''.5 \times 0''.4$  and is shown in the lower left.

For the 5, 8.4, and 15 GHz observations, after obtaining an image with a noise near but still well above the thermal limit, I subtracted the Fourier transform of B1849+005 from the visibility data, performed a modest amount of additional data editing, and then added the Fourier transform of B1849+005 back to the visibility data (Perley 1989). Figures 4–6 show the resulting images of B1849+005 between 5 and 15 GHz.

At 2.3 GHz, a significant detection of B1849+005 was obtained only on the shortest baseline, between the LA and PT antennas. As shown below, this source has a fairly simple structure on milliarcsecond scales. In order to estimate a diameter, the correlated visibility amplitude on the LA-PT baseline was compared to total flux density of the source. Furst et al. (1990) measure the flux density of the source at 2.7 GHz to be 0.77 Jy; flux densities obtained by interpolating its spectrum between 1.5 and 5 GHz (Fey et al. 1991; this work) range from 0.6 to 0.8 Jy. Because the measurement by Furst et al. (1990) utilized a single-dish telescope, I adopt 0.77 Jy as its flux density at 2.3 GHz. Assuming the source to be a circular Gaussian, its diameter is then 110 mas (Table 2).

For further analysis, the data were averaged in time. The averaging times were 30 s at 2.3 GHz, 60 s at 5 GHz, 30 s at 8.4 GHz, and 15 s at 15 GHz.

### 3. INTERSTELLAR SCATTERING TOWARD B1849+005

#### 3.1. Relevant Scattering Formulae

The interferometric visibility of an infinitely distant point source seen through a medium filled with random density fluctuations is

$$V(b) = e^{-D_\phi(b)/2} \quad (1)$$

for an interferometer with baseline length  $b$ . For the density power spectrum relevant in the interstellar medium (Armstrong

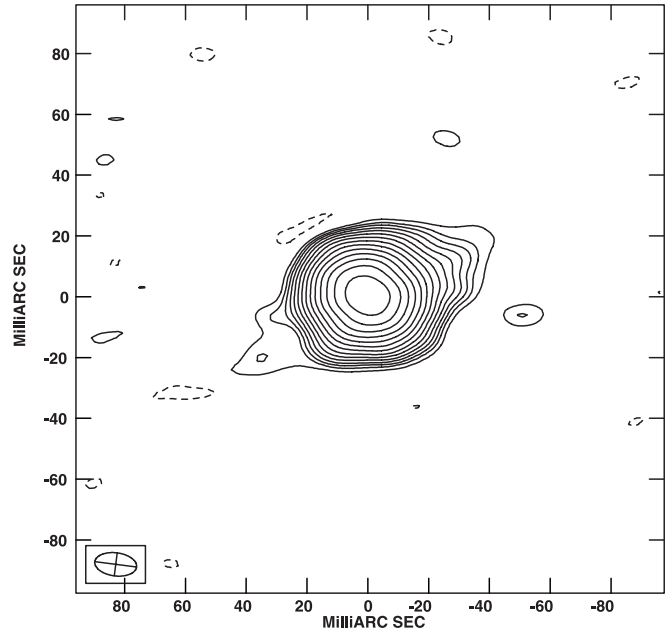


FIG. 4.—Central component of B1849+005 at 5 GHz, as observed by the VLBA. The rms noise level is  $0.39 \text{ mJy beam}^{-1}$ , and contour levels are  $0.39 \text{ mJy beam}^{-1} \times -2, 3, 5, 7.07, 10, \dots$ . The beam is  $14 \times 7.6 \text{ mas}$  and is shown in the lower left.

et al. 1995), the form of the phase structure function depends upon the value of the importance of  $l_1$  relative to the typical baseline length  $b$ . Anticipating later results, I consider two possibilities for  $D_\phi(b)$  (e.g., Coles et al. 1987; Cordes & Lazio 1991; Lambert & Rickett 1999)

$$D_\phi(b) = 8\pi r_e^2 \lambda^2 \text{ SM} \times \begin{cases} f(\alpha) b^{\alpha-2} & b \gg l_1, \\ f(\alpha) \Gamma(\alpha/2) l_1^{\alpha-2} [{}_1F_1(\alpha/2; 1; -(b/l_1)^2) - 1] & b \lesssim l_1. \end{cases} \quad (2)$$

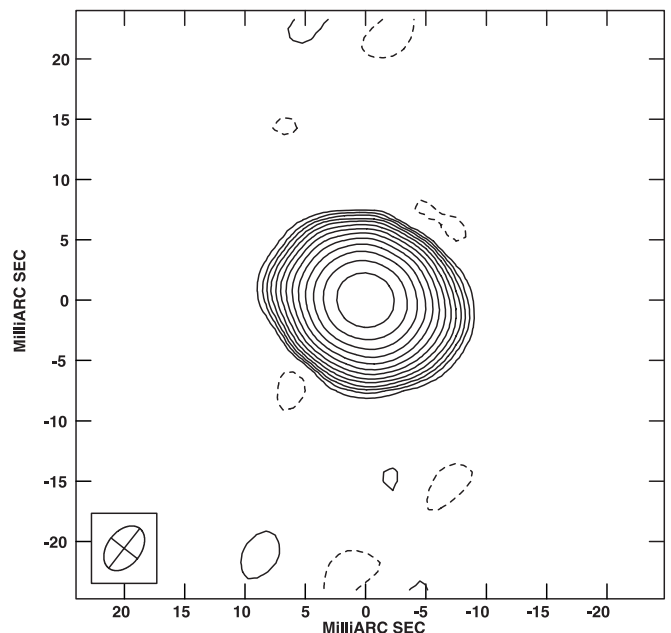


FIG. 5.—Central component of B1849+005 at 8.4 GHz. The rms noise level is  $0.51 \text{ mJy beam}^{-1}$ , and contour levels are  $0.51 \text{ mJy beam}^{-1} \times -3, 3, 5, 7.07, 10, \dots$ . The beam is  $4.2 \times 2.8 \text{ mas}$  and is shown in the lower left.

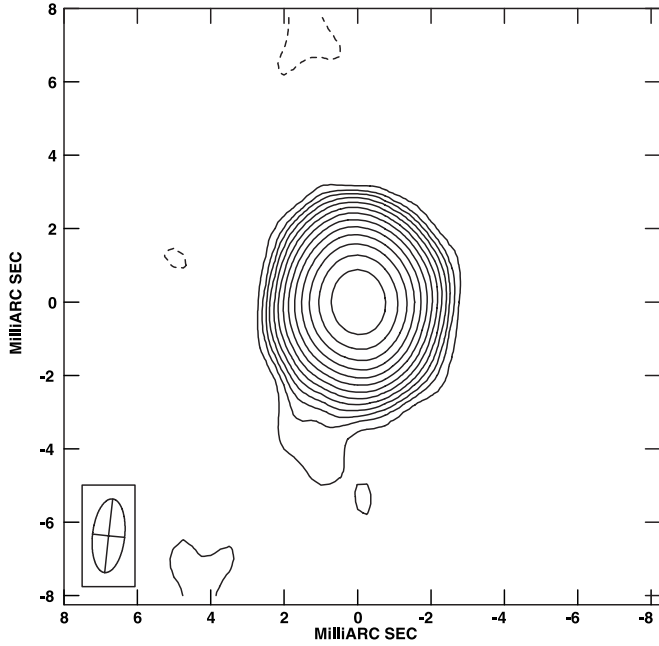


FIG. 6.—Central component of B1849+005 at 15 GHz. The rms noise level is  $0.84 \text{ mJy beam}^{-1}$ , and contour levels are  $0.84 \text{ mJy beam}^{-1} \times -2, 3, 5, 7.07, 10, \dots$ . The beam is  $2.0 \times 0.88 \text{ mas}$  and is shown in the lower left.

Here  $r_e$  is the classical electron radius,  $\lambda$  is the free-space observing wavelength,  $f(\alpha)$  is a slowly varying function of  $\alpha$  with a value near unity,  ${}_1F_1(a; b; x)$  is the confluent hypergeometric function, and the scattering measure SM is proportional to the line-of-sight integrated rms electron density. (Minor modifications are required if the source is not infinitely distant, as assumed here.) For reference, in the local interstellar medium,  $\text{SM} \approx 10^{-3.5} \text{ kpc m}^{-20/3}$  for a 1 kpc path length.

The resulting scattering diameter, for a distant source and assuming  $\alpha = 11/3$  (Rickett 1990; Cordes & Lazio 1991), is

$$\theta_d = \begin{cases} 128 \text{ mas SM}^{0.6} \nu_{\text{GHz}}^{-2.2} & b \gg l_1, \\ 71 \text{ mas SM}^{1/2} \nu_{\text{GHz}}^{-2} \left( \frac{l_1}{100 \text{ km}} \right)^{-1/6} & b \ll l_1, \end{cases} \quad (3)$$

where  $\nu_{\text{GHz}}$  is the observing frequency in GHz and SM is in its canonical units of  $\text{kpc m}^{-20/3}$ .

### 3.2. Angular Broadening and the Apparent Structure of B1849+005

On the basis of its spectrum, Fey et al. (1991) suggested that the structure of B1849+005 may be more complex than that of a single compact component. Figures 2 and 3 demonstrate that this is the case. Although a strong central component does dominate the structure of the source, there are weaker components both to the southwest and northeast. The components to the northeast are at best only faintly visible in the VLA observations at 4.9 GHz (Fig. 3), though their absence probably results from the limited hour-angle coverage and surface brightness sensitivity of the A-configuration of the VLA at this frequency. The central component may show a hint of a jet emerging to the southeast and bending toward the southwest. The existence of a jet must be considered tentative, however, given the extremely limited hour-angle coverage (only 1 minute observation). As the 0.33 GHz image is elongated in approximately the same orientation as that of the central and southwest components, I have also reimagined the (1998 March 19) 0.33 GHz observations utilizing superresolution. There is no indication of this second component, though the orientation of the beam is similar to that of the central and southwest components.

The expressions of § 3.1 assume an infinitely distant point source. To what extent can they be applied to B1849+005, given its complex structure? Figure 7 shows the diameter of the central component of B1849+005 as a function of observing frequency. Although Figures 1–6 show images of B1849+005, diameters measured from these images were not used in constructing Figure 7. Rather, Gaussian models were fitted to the visibility data, except in the case of the 2.3 GHz observations for which a circular Gaussian was assumed (§ 2). Also plotted in Figure 7 are measurements at various other frequencies. At these other frequencies (0.25 and 0.408 GHz) the visibility data were not available for analysis (as below), but angular diameters could be determined. For completeness, Table 2 summarizes the various fits for the diameter of the source.

Figure 7 also shows three curves,  $\theta \propto \nu^{-2.2}$ ,  $\theta \propto \nu^{-2}$ , and  $\theta \propto \nu^{-1.4}$ . The first two are relevant for strongly scattered sources, with the first being appropriate if the electron density

TABLE 2  
GAUSSIAN MODEL FITS TO THE CENTRAL COMPONENT OF B1849+005

Frequency (GHz)	$S$ (Jy)	$a$ (mas)	$b$ (mas)	$\Phi$ (deg)	References
0.25.....	$1.624 \pm 0.009$	$11,400 \pm 70$	$8430 \pm 60$	$44.2 \pm 0.7$	1
0.33.....	$2.1 \pm 0.2$	$6300 \pm 1000$	$2080 \pm 100$	$18 \pm 7$	2
0.33.....	$2.12 \pm 0.02$	$7050 \pm 350$	$2560 \pm 100$	$25.8 \pm 0.7$	2
0.41.....	$1.7 \pm 0.2$	$>600$	...	...	3
1.5 <sup>a</sup> .....	$0.63 \pm 0.06$	$440 \pm 6$	$190 \pm 6$	$161 \pm 1$	2
2.3.....	$0.77 \pm 0.1$	$110 \pm 5$	$110 \pm 5$	...	2
5.0.....	$0.739 \pm 0.009$	$19.34 \pm 1$	$17.32 \pm 1$	$27.0 \pm 0.6$	2
8.4.....	$0.634 \pm 0.006$	$6.71 \pm 0.3$	$4.91 \pm 0.2$	$-33.2 \pm 0.3$	2
15.....	$0.831 \pm 0.008$	$2.017 \pm 0.1$	$1.623 \pm 0.08$	$-21.1 \pm 0.5$	2

NOTES.—The visibility data are fit with a single Gaussian model having a flux density  $S$ , major axis  $a$ , minor axis  $b$ , and position angle  $\Phi$ . In some cases a circular Gaussian was fit; no position angle is reported for these cases. The first entry for 0.33 GHz is for the 1987 August 20 observations; the second is for the 1998 March 19 observations. The stated uncertainties are the formal statistical uncertainties for the fits; the actual uncertainties due to systematic effects are almost certainly larger.

<sup>a</sup> Only the central component was fitted.

REFERENCES.—(1) A. P. Rao (2002, private communication); (2) this work; (3) Dennison et al. (1984).

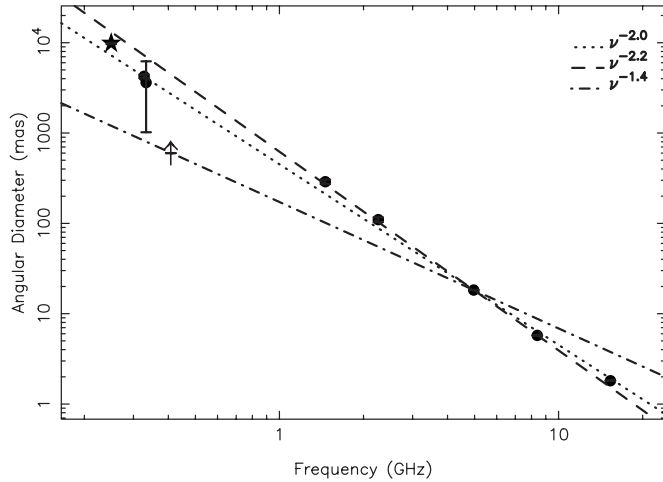


FIG. 7.—Angular diameter of B1849+005 as a function of observing frequency. The angular diameter was obtained by fitting a Gaussian either to the image or to the visibility; if an elliptical Gaussian was used in the fit, shown is the geometric mean of the major and minor axes. At most frequencies, the formal uncertainties are comparable to the size of the points. The datum at 0.25 GHz is from P. Rao (2001, private communication) and that at 0.408 from Dennison et al. (1984). For reference, three curves are also plotted, one showing a  $\nu^{-2}$  dependence for the diameter (dotted line), one showing a  $\nu^{-2.2}$  dependence (dashed line), and one showing a  $\nu^{-1.4}$  dependence (dot-dashed line) that would be expected if the angular broadening for B1849+005 is anomalous in a manner similar to that for PSR B1849+00 (§ 4.2). All three curves are constrained to go through the diameter measured at 5 GHz.

spectrum is a power law with a Kolmogorov spectral index,  $\alpha = 11/3$ , while the second is appropriate if the range of observing baselines is comparable to  $l_1$ . The third curve shows the frequency dependence for the angular broadening if scattering toward B1849+005 is anomalous in a manner similar to that seen for the pulsar PSR B1849+00 (§ 4.2). The relatively good agreement between the angular diameters and the first two curves is an indication that scattering dominates the apparent structure of the central component at least up to 15 GHz. Interpolating the angular diameter to the fiducial frequency of 1 GHz, the scattering diameter of B1849+005 is  $0''.6$ . Based on their more-limited set of observations, Fey et al. (1991) reached a similar conclusion: B1849+005 is heavily scattered but exhibits a more complex structure than simply a single compact component.

In addition, the angular diameter of the southwest component was measured, using the images shown in Figures 2 and 3. Its diameter is approximately constant between 1.5 and 4.9 GHz, indicating that its diameter is much larger than the scattering diameter. This is consistent with its somewhat diffuse appearance at 4.9 GHz.

### 3.3. The Electron Density Spectrum

A more profitable analysis of the observations is to use the structure function (eqs. [1]–[2]) to extract parameters of the electron density spectrum. My analysis follows closely that of Spangler & Cordes (1998). Figure 8 shows an example of a structure function constructed from the 8.4 GHz visibility data.

Clearly apparent in Figure 8 is a nonrandom scatter in the structure function, e.g., around 10 Mλ. Moreover, Figures 1 and 4–6 show that the scattered image has (varying) degrees of anisotropy. This anisotropy arises presumably because the density fluctuations responsible for the scattering are themselves anisotropic.

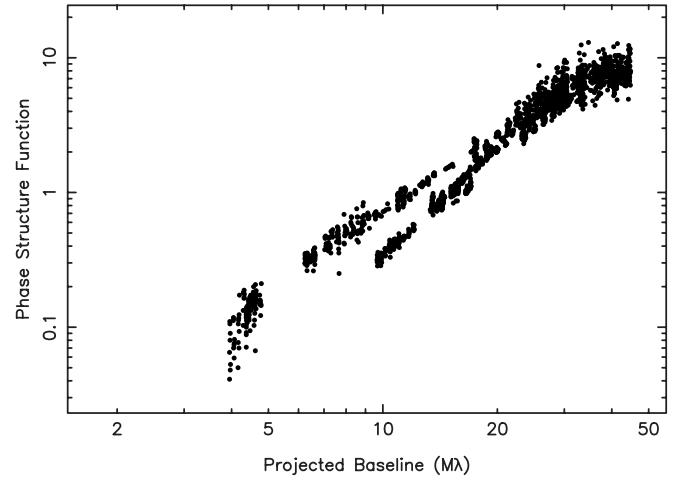


FIG. 8.—Structure function for the 8.4 GHz visibility data using the isotropic baseline. A small number of visibilities below 2 Mλ are not shown.

The anisotropy of the image and visibility data (and of the underlying density fluctuations) are described by an orientation  $\Psi$  and aspect ratio  $\eta$ . In fitting the visibility data to equation (1), the baseline  $b$  is replaced by the “rotundate” baseline

$$b_r^2 = (u \cos \Psi + v \sin \Psi)^2 + \eta^2 (-u \sin \Psi + v \cos \Psi)^2, \quad (4)$$

where  $u$  and  $v$  are the traditional interferometer baseline coordinates measured in units of the observing wavelength. The rotundate baseline is simply the baseline measured in an anisotropic coordinate system that is rotated relative to that of the interferometer’s coordinate system. In this rotundate coordinate system,  $\Psi$  is measured counterclockwise from the  $u$  axis, in contrast to the position image in an image, which is measured counterclockwise from north. Thus, there is a  $90^\circ$  offset from an image position angle and  $\Psi$ .

The nonrandom scatter in Figure 8 arises because of the use of the isotropic baseline ( $\eta = 1$  and  $\Psi = 0^\circ$ ). Figure 9 illustrates the use of the rotundate baseline in plotting the structure function (using the best-fitting power-law density spectrum model found below). Clearly apparent is the dramatic reduction in the scatter of the data; similar improvements are seen at the other frequencies. Figure 9 also demonstrates that the structure of B1849+005 does not have an adverse impact on efforts to extract information about the scattering. A single source component does an excellent job of fitting the visibilities. As might be expected from Figures 2 and 3, the VLBI observations are insensitive to the relatively low brightness temperature components to the southwest and northeast.

One important aspect of the use of the rotundate baseline is that the structure functions in equation (2) have been derived assuming an isotropic density spectrum. This *ex post facto* replacement of the rotundate baseline for the baseline violates that assumption. This replacement should be approximately valid provided that  $\eta$  is not much larger than unity. Moreover, Chandran & Backer (2002) have considered the propagation of radio waves through an anisotropic medium. They find that expressions like those of equation (2) continue to hold; in particular, the power-law dependences remain unchanged.

Using rotundate baselines and the structure functions of equation (2), there are four or five parameters for which to fit, depending upon the relative importance of the inner scale:  $\alpha$ ,

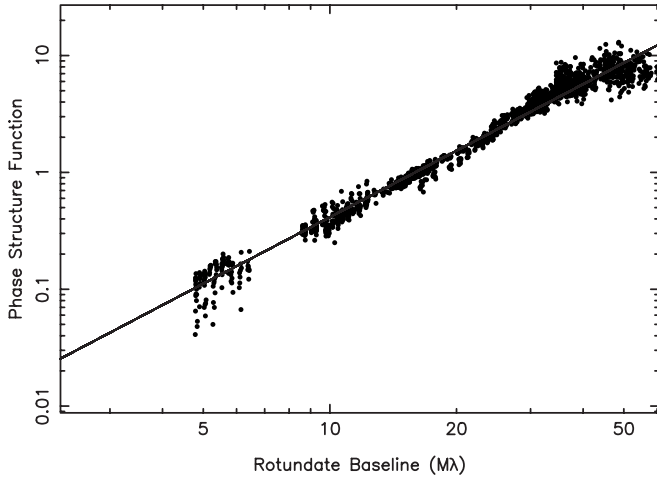


FIG. 9.—Structure function for the 8.4 GHz visibility data using the rotundate baseline. The solid line shows the best-fitting model for a power-law density spectrum (viz., Table 3). A small number of visibilities below 2 Mλ are not shown.

SM,  $\eta$ ,  $\Psi$ , and  $l_1$ . I used a genetic algorithm (Lazio 1997) to find the best-fitting parameters in a (unweighted) minimum  $\chi^2$  sense at each frequency.

I have fit the structure functions (as in Fig. 8) for the VLBI observations (2.3–15 GHz) and the 0.33 GHz VLA observations of 1998 March 19. The visibility data from the 1.5 or 4.9 GHz observations from the VLA were not used, because it is clear that the source structure is complex, and at 4.9 GHz,

the expected scattering diameter is much smaller than what can be resolved by the VLA. In addition, the 0.33 GHz visibility data from the 1987 August 20 VLA observations were not used because of their limited quantity and restricted  $u$ - $v$  coverage.

Not all of the data were used in the fitting. At long baselines, the structure functions saturate, while at short baselines they reach noise plateaus (viz., eqs. [1] and [2]). The saturation at long baselines is visible near 30 Mλ in Figures 8 and 9; the noise plateau at short baselines occurs below 2 Mλ (for the 8.4 GHz data). Consequently, limits were set at both short and long baselines. After excluding noisy data, the total number of data available to fit ranged from several hundred to several thousand.

Figures 10 and 11 show the best-fitting parameters and their confidence ranges as a function of frequency for both a power-law density spectrum ( $b \gg l_1$ ) and a density spectrum with an inner scale ( $b \lesssim l_1$ ), respectively; Tables 3 and 4 tabulate the best-fitting model parameters. Figures 10 and 11 also indicate the (weighted) mean values, over all frequencies, for the various parameters. A  $\chi^2$  statistic was used to test whether the best-fit values are consistent with a single mean value, i.e., no frequency dependence.

The confidence ranges for the parameters have been estimated both by a local grid search and a nonlinear least-squares minimization around the minimum  $\chi^2$ . In the former method, the confidence range for a parameter was determined by varying that parameter, while holding all others fixed at their best-fitting values, until the  $\chi^2$  approximately doubled from its minimum value. In the latter method a Levenberg-Marquardt minimization routine was used to determine the covariance

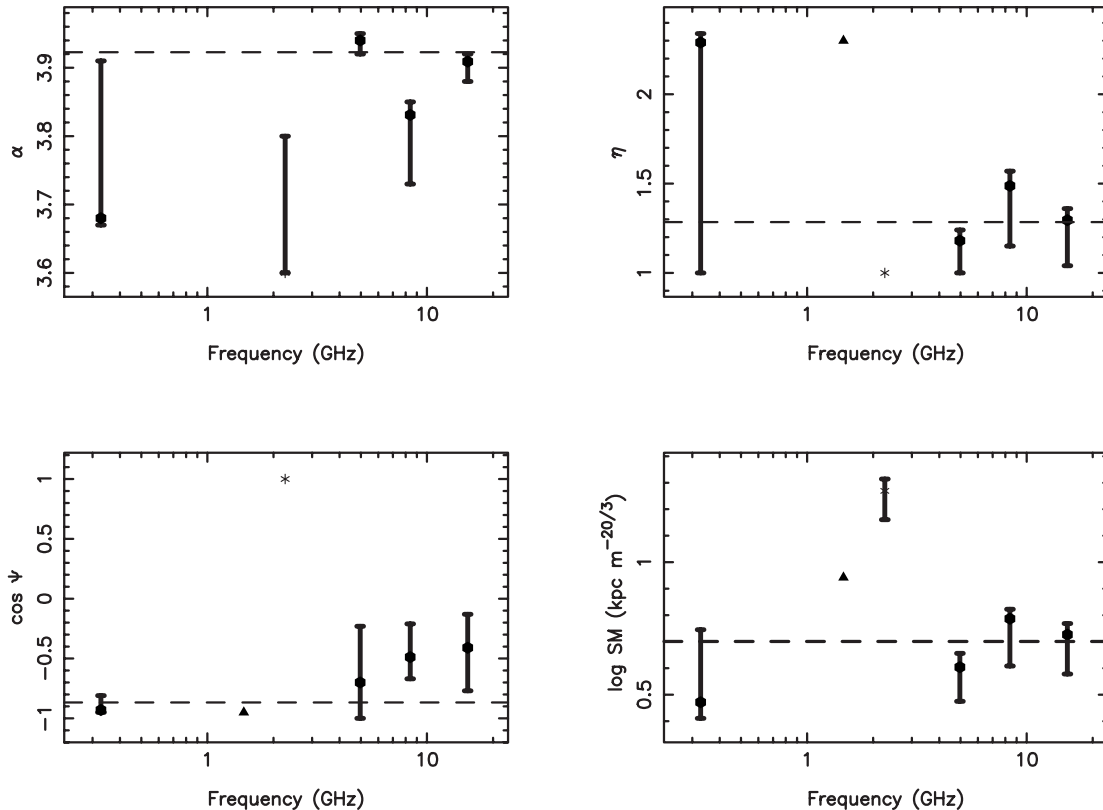


FIG. 10.—Best-fit parameters as a function of frequency for a power-law density spectrum. The confidence regions shown are the amount by which the parameter must change in order to cause the  $\chi^2$  to increase by unity from its minimum value. The horizontal dotted line shows the weighted mean value for the parameter. Because B1849+005 was detected on only a single baseline at 2.3 GHz (*asterisk*), the anisotropy  $\eta$  and its orientation  $\Psi$  were constrained to be 1 and 0 ( $\cos \Psi = 1$ ), respectively. At 1.5 GHz, a structure function analysis was not conducted; the values shown are derived from analysis of the image (*triangle*).

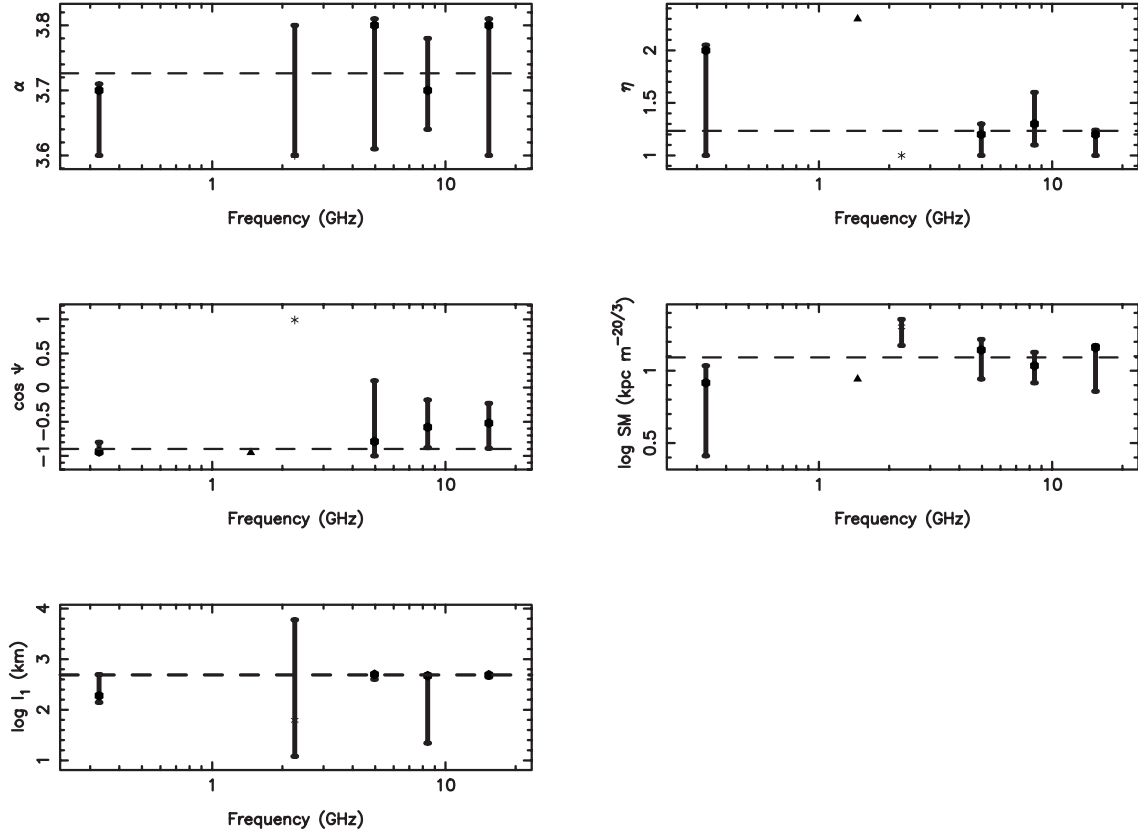


FIG. 11.—Same as Fig. 10, but for best-fit parameters as a function of frequency for a density spectrum with an inner scale.

matrix of the parameters. The Levenberg-Marquardt minimization yields confidence ranges much smaller than the grid search. We have adopted the confidence ranges for the grid search; adopting smaller confidence ranges would make our following conclusions more robust.

One aspect of Figures 10 and 11 warrants comment. The various parameters ( $\alpha$ , SM,  $\eta$ ,  $\Psi$ , and  $l_1$ ) are plotted as functions of frequency. These parameters were introduced as frequency-independent quantities (eq. [2]). For instance, SM is proportional to the rms electron density. The apparent frequency dependence arises from the use of interferometers whose baseline lengths were not scaled with frequency. For an interferometer with a typical (and fixed) baseline length  $b$ , it will resolve the scattering disk only if the scattering disk is comparable in size to the typical angle measured by the interferometer  $\lambda/b$ . In turn, if the scattering medium is at a

distance  $D$ , the scattering disk will be produced by density fluctuations on scales of  $l' \sim D(\lambda/b)$ . This length scale is manifestly frequency dependent. Thus, an apparent frequency dependence in  $\alpha$ , SM,  $\eta$ ,  $\Psi$ , or  $l_1$  would reflect different parameter values being obtained on different length scales within the spectrum of scattering irregularities. For brevity, in the context of Figures 10 and 11, I shall continue to speak of a frequency dependence for  $\alpha$ , SM,  $\eta$ ,  $\Psi$ , and  $l_1$  with the understanding that any frequency dependence arises from the different length scales probed in the scattering medium.

### 3.3.1. Image Anisotropy

Regardless of whether a power-law or inner-scale density spectrum is fitted to the structure functions, the result confirms what the casual inspection of Figures 1–6 suggest: the scattering toward B1849+005 is decidedly anisotropic.

At 0.33 GHz, the anisotropy appears large,  $\eta \simeq 2.3$ , but the weaker components, especially the one to the southeast, may

TABLE 3  
POWER-LAW DENSITY SPECTRUM MODEL FITTING

Frequency (GHz)	$\alpha$	$\eta$	$\Psi$ (deg)	log SM (kpc m <sup>-20/3</sup> )
0.33.....	3.68 <sup>+0.23</sup> <sub>-0.01</sub>	2.29 <sup>+0.05</sup> <sub>-1.3</sub>	158 <sup>+4</sup> <sub>-14</sub>	0.47 <sup>+0.41</sup> <sub>-0.06</sub>
1.5 <sup>a</sup> .....	...	2.3	161	0.98
2.3 <sup>b</sup> .....	3.60	...	...	1.3
5.0.....	3.94 <sup>+0.01</sup> <sub>-0.02</sub>	1.18 <sup>+0.06</sup> <sub>-0.18</sub>	134 <sup>+46</sup> <sub>-31</sub>	0.60 <sup>+0.08</sup> <sub>-0.15</sub>
8.4.....	3.83 <sup>+0.02</sup> <sub>-0.10</sub>	1.49 <sup>+0.08</sup> <sub>-0.34</sub>	119 <sup>+13</sup> <sub>-17</sub>	0.79 <sup>+0.08</sup> <sub>-0.26</sub>
15.....	3.91 <sup>+0.01</sup> <sub>-0.03</sub>	1.29 <sup>+0.07</sup> <sub>-0.25</sub>	114 <sup>+26</sup> <sub>-17</sub>	0.73 <sup>+0.07</sup> <sub>-0.21</sub>
Mean .....	3.92	1.30	141	0.68

<sup>a</sup> At this frequency, the scattering parameters were derived from the image, not from a structure function analysis.

<sup>b</sup> At this frequency, the scattering diameter was assumed to be circular.

TABLE 4  
POWER-LAW WITH INNER-SCALE DENSITY SPECTRUM MODEL FITTING

Frequency (GHz)	$\alpha$	$\eta$	$\Psi$ (deg)	log SM (kpc m <sup>-20/3</sup> )	$l_1$ (km)
0.33.....	3.70 <sup>+0.01</sup> <sub>-0.10</sub>	2.00 <sup>+0.05</sup> <sub>-1.0</sub>	160 <sup>+4</sup> <sub>-17</sub>	0.92 <sup>+0.28</sup> <sub>-0.63</sub>	190 <sup>+310</sup> <sub>-50</sub>
2.3 <sup>a</sup> .....	3.60	...	...	1.30 <sup>+0.1</sup> <sub>-0.1</sub>	62 <sup>+12</sup> <sub>-12</sub>
5.0.....	3.80 <sup>+0.01</sup> <sub>-0.19</sub>	1.20 <sup>+0.10</sup> <sub>-0.20</sub>	142 <sup>+38</sup> <sub>-58</sub>	1.14 <sup>+0.21</sup> <sub>-0.42</sub>	500 <sup>+0</sup> <sub>-100</sub>
8.4.....	3.70 <sup>+0.08</sup> <sub>-0.06</sub>	1.30 <sup>+0.30</sup> <sub>-0.20</sub>	125 <sup>+26</sup> <sub>-25</sub>	1.03 <sup>+0.25</sup> <sub>-0.25</sub>	470 <sup>+30</sup> <sub>-448</sub>
15.....	3.80 <sup>+0.01</sup> <sub>-0.20</sub>	1.20 <sup>+0.04</sup> <sub>-0.20</sub>	121 <sup>+32</sup> <sub>-18</sub>	1.16 <sup>+0.04</sup> <sub>-0.58</sub>	490 <sup>+10</sup> <sub>-50</sub>
Mean .....	3.78	1.23	148	1.14	470

<sup>a</sup> At this frequency, the scattering diameter was assumed to be circular.

be contaminating the analysis. The beam diameter at 0.33 GHz is comparable to the separation between the components, and the orientation of the source at 1.5 GHz is similar to that of both the source and the position angle of the beam at 0.33 GHz. The visibilities at 0.33 GHz appear consistent with only a single component being present (§ 3.2 and Fig. 7), but the presence of the other components cannot be excluded. Indeed, convolving the 1.5 GHz image, Figure 2, to a resolution comparable to that of the 0.33 GHz images, Figure 1, produces an image similar to the 0.33 GHz images.

Even if the analysis at 0.33 GHz is disregarded (and at 1.5 and 2.3 GHz, for which less comprehensive analyses could be performed), the higher-frequency data show a clear anisotropy. The fits at 5.0 and 15 GHz are just marginally consistent with an isotropic image, while the fit at 8.4 GHz excludes an isotropic image. The mean value for the image elongation is  $\bar{\eta} = 1.2$ . This value is comparable to that measured for Cyg X-3 ( $\approx 1.3$ , Wilkinson et al. 1994; Molnar et al. 1995) and NGC 6334B (1.2–1.5; Trotter et al. 1998), within the range of anisotropies measured for the extragalactic sources seen through the Cygnus region (1.1–1.8; Spangler & Cordes 1988, 1998; Desai & Fey 2001), and somewhat smaller than the value measured for the OH masers toward W49N (2–3; Desai et al. 1994) and the Galactic center ( $\approx 2.5$ ; Frail et al. 1994). Romani et al. (1986) have predicted the anisotropy that would be induced, even if the small-scale (diffractive) density fluctuations responsible for angular broadening are isotropic, by refractive effects from large-scale density fluctuations. For a thin scattering screen with a Kolmogorov density spectrum, the expected anisotropy is  $\langle \eta \rangle < 1.05$ . The scattering toward B1849+005 is both strong and anisotropic, and the anisotropy must result from the density fluctuations responsible for the scattering.

Whether the position angle  $\Psi$  of the anisotropy changes with frequency, as Wilkinson et al. (1994) and Trotter et al. (1998) found for Cyg X-3 and NGC 6334B, respectively, is less certain. In both Figures 10 and 11, an apparent trend of a decreasing position angle (or increasing  $\cos \Psi$ ) is seen. This is the case regardless of whether the 0.33 GHz datum is included or not. However, as both figures show, the uncertainties are also consistent with no change in position angle.

Using only the higher-frequency data, the scattering diameter of B1849+005 ranges from 19 mas at 5.0 GHz to 2 mas at 15 GHz. If the material responsible for the scattering is at a distance of 5 kpc (§ 4.2), the size of the region on which the anisotropic density fluctuations occur must range from  $1.5 \times 10^{14}$ – $1.4 \times 10^{15}$  cm (10–95 AU). These scales are comparable to those seen for NGC 6334B, though this is due partially to a selection effect in that the same telescope was used in both this work and that of Trotter et al. (1998), so the range of accessible spatial scales is the same.

Within the context of the models for magnetohydrodynamic turbulence developed by Goldreich and collaborators (e.g., Lithwick & Goldreich 2001), these length scales would represent the lower limit to their “MHD scale.” On this length scale, the kinetic energy density ( $\propto v^2$ ) of the turbulent eddies has diminished to the point that the magnetic energy density ( $\propto B^2$ ) is comparable to it. Thus, this length scale marks where the turbulence makes a transition from isotropic on large scale (comparable to the outer scale) to increasingly anisotropic on small scales.

### 3.3.2. Inner Scale

Comparison of Figures 10 and 11 shows that the density spectral index  $\alpha$  appears to change between 0.33 and 5.0 GHz

for the power-law spectrum. At 0.33 GHz, the fit for a power-law spectrum finds  $\alpha = 3.68$ , while above 5.0 GHz,  $\alpha > 3.8$ . In contrast, the fit for an inner-scale spectrum reveals a much more consistent set of values for  $\alpha$ , with  $3.7 < \alpha < 3.8$ . Moreover, the fits for the inner scale itself find consistent values of a few hundred kilometers (though with large uncertainties).

I regard this as a detection of the effects of the inner scale on scales of a few hundred kilometers. The maximum baselines of the VLA, used for the 0.33 GHz observation, are 35 km. In contrast, the VLBA baselines, used for the higher-frequency observations, span the range from a few hundred to a few thousand kilometers. Thus the “break” between 0.33 and 5.0 GHz in the fits for  $\alpha$  in the power-law density spectrum (Fig. 10) reflects the range of baselines used in the observations.

This value for the inner scale, a few hundred kilometers, is comparable to that found toward other sources (Spangler & Gwinn 1990; Moran et al. 1990; Wilkinson et al. 1994; Molnar et al. 1995).

### 3.4. Secular Change of the Scattered Image

If the plasma responsible for the scattering has a bulk (transverse) velocity  $v$  (and it remains relatively unchanged as it moves across the line of sight, “frozen-flow” approximation), changes in the image appearance should appear on timescales comparable to the refractive timescale  $t_r = l_r/v$ . The two observations at 0.33 GHz (Fig. 1) provide a 10.6 yr baseline over which to search for secular changes in the image.

Table 2 shows that both the fitted diameters and position angles for the source do not change appreciably. From both sets of observations  $\theta_d \approx 4''$  at 0.33 GHz. The refractive scale is therefore  $6 \times 10^{16}$  cm  $D_{\text{kpc}}$ , where  $D_{\text{kpc}}$  is the distance to the screen in kiloparsecs. There is little change in the image over the 10.6 yr interval. The velocity of the scattering material is therefore  $v \leq 1800$  km  $s^{-1}$   $D_{\text{kpc}}$ . (Strictly, this velocity is a combination of the velocities of the source, medium, and observer. Here the velocity of the source is assumed to be effectively zero.)

This upper limit is conservative. If the actual velocity were within a factor of two, say, of this upper limit, some modest changes in at least the orientation should start to become apparent.

The source B1849+005 is only 14' from the supernova remnant (SNR) G33.6+0.1. Spangler et al. (1986) observed B1849+005 with the aim of assessing to what extent the SNR could contribute to the scattering of B1849+005. While they inferred correctly that B1849+005 is heavily scattered, they were reluctant to attribute all of the scattering to G33.6+0.1 given the low-latitude line of sight to B1849+005. Unfortunately, this upper limit on the velocity of the scattering material sheds no light on whether material from the SNR is responsible for the scattering. The large scattering diameter at 0.33 GHz means that relatively large length scales are probed within the scattering material and that correspondingly long time intervals are needed to place stringent constraints on the velocity.

The higher-frequency VLBI observations may prove useful in constraining the velocity of the scattering material in the future. For instance, repeating the 8.4 GHz observations after a 7 yr interval would place a 5 km  $s^{-1}$  limit on the velocity (presuming that no change in the scattering disk was seen).

## 4. THE SCATTERING ENVIRONMENT AROUND B1849+005

### 4.1. Nearby Lines of Sight

By virtue of the VLA's large field of view at 0.33 GHz ( $\approx 2.5^\circ$ ), other highly scattered sources may be detectable in the

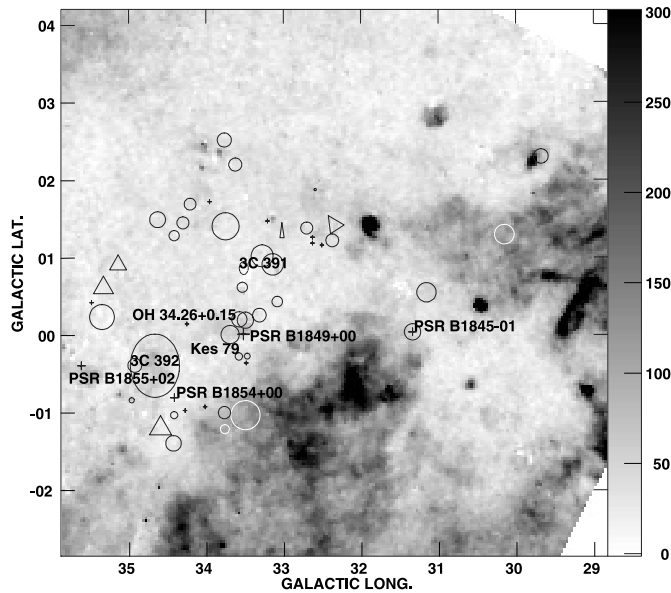


FIG. 12.—Lines of sight in the 0.33 GHz field of view of B1849+005 that may also be dominated by scattering. The gray scale shows the smoothed, continuum-subtracted H $\alpha$  emission from the Southern H-Alpha Sky Survey Atlas (Gaustad et al. 2001) on a linear scale from 0 to 30 Rayleighs. Sources marked with crosses appear unresolved; sources marked by circles appear resolved, with simple structure indicating that scattering probably dominates; and sources marked by triangles indicate sources whose structures may be more complex and therefore contain contributions from both scattering and intrinsic structure. The size of a circle or triangle is proportional to the source's diameter at 0.33 GHz. Sources identified are the pulsars PSR B1849+00, PSR B1854+00, PSR B1855+02, the supernova remnants Kes 79, 3C 391 and 3C 392, and the maser OH 34.26+0.15. The source B1849+005 is just above PSR B1849+00 (viz., Fig. 13).

direction of B1849+005. With only a single frequency, I cannot demonstrate unambiguously that scattering dominates the structure of other sources in the field. However, given that B1849+005 and PSR B1849+00 (see following section) are both highly scattered and that PSR B1845-01 also exhibits a large amount of pulse broadening (Ramachandran et al. 1997), it is reasonable to consider that scattering may contribute to the observed diameters of many of these sources.

Figure 12 shows the angular diameters for all sources in the 0.33 GHz field of view of B1849+005 that are judged to be compact and likely dominated by scattering. Table 5 tabulates the diameters of these sources.

If the structures of these sources are dominated by scattering, there is substantial variation in the scattering on sub-degree angular scales. Slysh et al. (2001) have reached a similar conclusion by comparing their space VLBI observations of the maser OH 34.26+0.15 to scattering measurements for PSR B1849+00 and B1849+005. They find the maser to have an angular diameter of less than 1 mas, from which they deduce a scattering measure of  $1.68 \times 10^{-3} \text{ kpc m}^{-20/3}$ , far less than that of PSR B1849+00 or B1849+005, though in this case it is likely that the maser lies in front of the strong scattering region.

Figure 12 suggests that the region of intense, yet spatially variable scattering may subtend a large angle on the sky. For instance, there are a number of sources near (18<sup>h</sup>47<sup>m</sup>5, +2°) whose diameters range from unresolved to 7". Numerous other cases of unresolved sources fairly close to sources with measurable diameters also can be identified. These lines of sight may be similar to other directions showing both heavy and anisotropic scattering and large changes in the scattering

strength on degree size scales such as the Cygnus region (Fey et al. 1989; Lazio et al. 1990; Spangler & Cordes 1998; Desai & Fey 2001), the Galactic center (van Langevelde et al. 1992; Frail et al. 1994), and along the Galactic plane (Dennison et al. 1984; Fey et al. 1991).

#### 4.2. The Line of Sight to PSR B1849+00

The pulsar PSR B1849+00 is only 13' from B1849+005 and is the most heavily scattered pulsar known, with a pulse broadening time of 0.2 seconds at 1.4 GHz. Löhmer et al. (2001) show that between 1.4 and 2.7 GHz the pulse broadening of this pulsar is anomalous in the sense that its frequency dependence is  $\nu^{-x}$  with  $x = 2.8^{+1.0}_{-0.6}$  rather than the expected  $x \approx 4$ . In turn, this anomalous frequency scaling implies a density spectral index of  $\alpha = 6.6^{+7.8}_{-2.3}$ . (For a review of other observations of this pulsar, see Stanimirovic et al. 2003.)

My observations of B1849+005 are at frequencies that bracket those used by Löhmer et al. (2001) to observe PSR B1849+00 (Fig. 7). Unfortunately, the large uncertainties on the angular diameters between 0.33 and 2.3 GHz preclude definite conclusions about the possibility of similar anomalous scattering along the line of sight to B1849+005. On the one hand, the frequency scaling for the angular diameter between 1.5 and 2.3 GHz is  $\nu^{-2.3}$  and the frequency scaling between 0.33 and 5 GHz is  $\nu^{-2}$ . Both of these frequency scalings (as well as Fig. 7) would suggest a frequency dependence of approximately  $\nu^{-2}$  is a much better description for the angular broadening than a dependence of approximately  $\nu^{-1.4}$  (because the pulse broadening and angular broadening are related as  $\tau \sim \theta^2$ ). Recall, though, that the 0.33 GHz diameter may be overestimated because of contamination from the source structure (§ 3.2), the 1.5 GHz diameter is somewhat smaller than the resolution of the array, and at 2.3 GHz the diameter has been estimated from only a single baseline.

Cordes & Lazio (2001; their Figs. 2 and 3) showed that anomalous pulse broadening, over a limited frequency range and possibly consistent with that observed by Löhmer et al. (2001), can be produced by two scattering screens having different scattering strengths. Such a scenario would produce anomalous angular broadening as well. I model this anomalous scattering in a piecewise linear fashion, with angular broadening scaling approximately as  $\nu^{-2.2}$  below 1.4 GHz and above 2.7 GHz, while between 1.4 and 2.7 GHz it would scale as  $\nu^{-1.4}$ . This model produces an overall frequency scaling between 0.33 and 5 GHz of  $\nu^{-1.9}$ . Thus, while Figure 7 shows that the angular diameter appears to scale as expected with frequency, a modest amount of anomalous scattering at frequencies near 1.5 GHz cannot be excluded.

A more stringent constraint on the anomalous scattering of PSR B1849+00 could be obtained from multifrequency observations of its angular diameter. The field of view of the VLA is sufficiently large that PSR B1849+00 is detected in both the 0.33 and 1.5 GHz observations. Unfortunately, at 0.33 GHz it is unresolved, while at 1.5 GHz it is sufficiently near the edge of the primary beam that it is difficult to obtain a reliable angular-diameter estimate. VLBI observations are under way (and will be reported elsewhere) to observe B1849+005 and PSR B1849+00 simultaneously near 1.5 GHz in an effort to see if the pulsar's angular diameter appears anomalous.

Nonetheless, by combining the various observations for B1849+005 and PSR B1849+00, it may be possible to constrain the properties of the regions responsible for the excess scattering. The scattering toward B1849+005 and PSR B1849+00

TABLE 5  
OTHER POSSIBLY SCATTERED SOURCES NEAR B1849+005

Right Ascension	Declination	Galactic Longitude (deg)	Galactic Latitude (deg)	Diameter (arcsec) (5)	Structure (6)
18 35 10.617.....	01 45 52.86	32.650	4.422	...	?
18 37 18.258.....	−01 50 26.68	29.680	2.302	3.8	
18 41 44.789.....	−01 52 52.35	30.152	1.297	5.1	
18 43 58.583.....	01 53 27.68	33.766	2.522	3.7	
18 44 07.675.....	00 33 17.10	32.592	1.879	0.6	
18 44 50.864.....	01 37 15.89	33.624	2.205	3.4	
18 45 17.789.....	00 07 42.94	32.117	1.308	5.2	?
18 46 03.708.....	00 03 39.24	32.265	1.168	3.3	
18 46 05.681.....	00 25 38.53	32.703	1.384	3.1	
18 46 14.538.....	−01 19 40.83	31.158	0.550	5.0	
18 46 23.171.....	00 18 28.74	32.630	1.264	...	
18 46 31.286.....	00 09 08.35	32.507	1.163	...	
18 46 39.510.....	00 16 23.36	32.630	1.188	...	
18 46 41.266.....	00 55 14.98	31.571	0.637	...	
18 46 53.543.....	00 41 02.80	33.023	1.323	2.6	?
18 47 09.999.....	01 41 55.15	33.957	1.724	...	
18 47 43.843.....	01 54 33.63	34.209	1.695	3.0	
18 47 55.076.....	01 22 19.10	33.752	1.409	7.0	
18 48 23.488.....	−01 23 58.55	31.339	0.039	4.2	
18 48 25.281.....	00 46 36.09	31.897	0.317	5.7	
18 48 34.187.....	00 36 18.25	32.067	0.362	5.5	
18 48 45.681.....	01 52 55.68	34.302	1.453	3.1	
18 49 12.392.....	02 11 32.05	34.629	1.496	4.1	
18 49 33.461.....	01 54 29.11	34.416	1.288	2.6	
18 50 10.398.....	00 20 04.02	33.086	0.434	2.7	
18 50 20.140.....	00 49 13.91	33.537	0.619	2.6	
18 50 40.088.....	03 57 33.61	36.370	1.975	2.4	
18 51 12.962.....	00 27 37.89	33.317	0.259	3.5	
18 51 52.819.....	00 40 01.42	32.389	−0.403	3.9	
18 52 12.978.....	02 22 52.19	35.140	0.912	5.1	?
18 52 27.364.....	00 32 00.70	33.523	0.017	...	
18 53 23.434.....	00 21 37.42	32.834	−0.599	1.5	
18 53 36.039.....	00 27 14.06	32.775	−0.688	1.9	
18 53 37.212.....	02 24 56.68	35.331	0.616	6.0	?
18 53 43.689.....	00 19 56.05	33.489	−0.358	...	
18 54 34.997.....	02 27 51.16	35.484	0.424	...	
18 54 59.951.....	02 15 39.94	35.350	0.239	6.4	
18 56 09.016.....	00 02 04.43	33.500	−1.033	7.5	
18 56 27.229.....	01 35 57.48	34.927	−0.386	3.6	
18 56 31.711.....	00 17 27.47	33.771	−1.000	3.2	
18 56 43.059.....	00 32 50.93	34.021	−0.925	...	
18 57 16.674.....	00 11 21.39	33.766	−1.213	2.3	
18 57 21.043.....	00 45 28.03	34.281	−0.970	...	
18 57 49.365.....	00 51 17.91	34.421	−1.031	1.8	
18 58 07.936.....	01 25 49.86	34.969	−0.837	1.3	
18 58 44.966.....	00 55 59.52	34.596	−1.201	6.6	?
18 59 08.028.....	00 41 48.99	34.430	−1.394	4.0	

NOTES.—Units of right ascension are hours, minutes, and seconds, and units of declination are degrees, arcminutes, and arcseconds in J2000 coordinates. Col. (5): unresolved sources noted with ellipses (...). Col. (6): question mark indicates whether a visual inspection of the source image suggests a contribution from intrinsic structure to the measured angular diameter.

is a factor of 5 or more in excess of what is predicted by the large-scale components (a thick disk, thin disk, and spiral arms) of the Cordes-Lazio model (and the model by Taylor & Cordes 1993). In order to reproduce the observed scattering toward PSR B1849+00, Cordes & Lazio (2003) introduced a “clump” or “cloud” of electrons along the line of sight to it. They require the clump to have an internal electron density  $n_e = 10 \text{ cm}^{-3}$  and a fluctuation parameter  $F = 200$ . The fluctuation parameter  $F$  (see also Cordes et al. 1991) is a combination of the fractional variation of the electron density internal to the clump and the

outer scale. Larger values of  $F$  mean that a clump is more efficient at scattering. (For a clump, the fluctuation parameter and the scattering measure are proportional,  $\text{SM} \propto F n_e^2 \Delta r$ , where  $\Delta r$  is the size of the clump.) They placed the clump at a distance of 7.4 kpc and assumed its size to be  $\Delta r = 20 \text{ pc}$ .

The power of combining the measurements is twofold. First, the magnitude of angular broadening is strongly dependent upon the distribution of scattering material along the line of sight, with material close to the observer contributing more strongly (van Langevelde et al. 1992; Lazio & Cordes

1998). Consider a Galactic source at a distance  $D$  with angular broadening  $\theta_{\text{Gal}}$  and an extragalactic source along a similar line of sight with angular broadening  $\theta_{\text{xgal}}$ . If the scattering along the line of sight is dominated by a single screen at a (radial) distance  $\Delta$  from the Galactic source, then (van Langevelde et al. 1992)

$$\frac{\theta_{\text{Gal}}}{\theta_{\text{xgal}}} = \frac{\Delta}{D}. \quad (5)$$

This relationship implies that, even though seen through the same scattering screen, a Galactic source will have a smaller scattering diameter than an extragalactic source; this result occurs because the scattering screen is less effective at scattering the diverging wavefronts from the Galactic source than the planar wavefronts from the extragalactic source.

The 0.33 GHz scattering diameter of B1849+005 is  $4''.2$ . Taking an upper limit on the scattering diameter of PSR B1849+00 to be  $3''$  ( $=1/2$  the beam diameter),  $\Delta/D < 0.7$ . As PSR B1849+00 is at a distance of roughly 8 kpc,  $\Delta < 5.7$  kpc, or the scattering screen must be more than 2.3 kpc from the Sun.

The second reason for combining the measurements toward B1849+005 and PSR B1849+00 is that angular broadening and pulse broadening have different weightings for the distribution of scattering material along the line of sight. If  $x$  is the fractional distance between the pulsar and the observer (with  $x = 0$  being at the pulsar and  $x = 1$  being at the observer), then pulse broadening is weighted as  $x(1-x)$ , while angular broadening is weighted as  $x^2$ .

I have repeated the analysis of Cordes & Lazio (2003) but now requiring that a single clump describe the excess scattering toward both PSR B1849+00 and B1849+005. Specifically, I adopt the large-scale components of the Cordes-Lazio model and then search for a clump of excess scattering that can explain the observed scattering diameter for B1849+005, the upper limit on the scattering diameter of PSR B1849+00, and the pulse broadening of PSR B1849+00. A grid search over the three parameters  $n_e$ ,  $F$ , and  $x$  was used to search for the best fit in a minimum  $\chi^2$  sense. The size of the clump is assumed to be 40 pc, so that it covers both lines of sight even when the clump is near the pulsar.

An added constraint in the fitting process is that the dispersion measure of the pulsar ( $\text{DM} = 680 \text{ pc cm}^{-3}$ ) and the modeled distance to the pulsar must be self-consistent. That is, increasing the density within the clump necessarily reduces the modeled distance to the pulsar, which in turn affects the weighting for the scattering observables. The fitting procedure was therefore the following. The dispersion measure contributed by the clump,  $\delta\text{DM}$ , was determined for each set of values for  $n_e$  and  $x$ . The model distance for the pulsar was determined by requiring that the large-scale components of the Cordes-Lazio model account for the remainder of the pulsar's DM, i.e., for  $(\text{DM} - \delta\text{DM})$ . This new distance was then used in determining the weighting factors for the modeled scattering observables. In practice, the  $\delta\text{DM}$  contributed by the clump is sufficiently small that it does not affect the modeled pulsar distance ( $\approx 9$  kpc) significantly.

No set of parameters can reproduce all three observational constraints. In particular, the pulsar's pulse broadening is consistently underestimated (by about an order of magnitude), while the extragalactic source's angular diameter is overestimated (by about a factor of 2–3). As might be expected, because the observational constraints are all due to scattering,

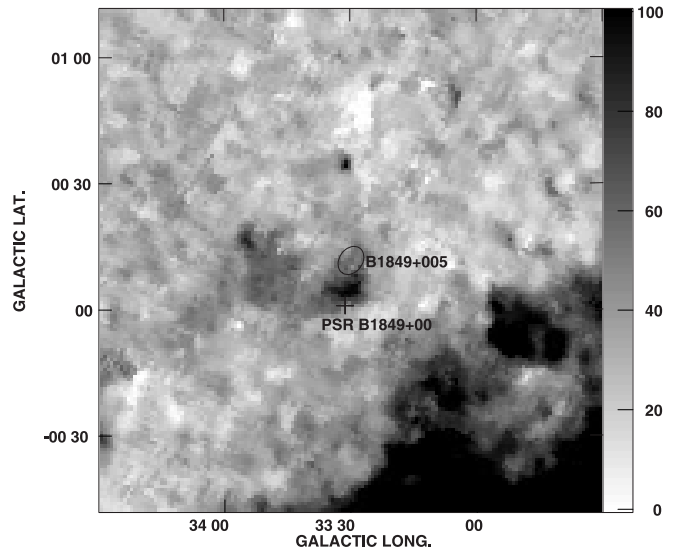


FIG. 13.—Subimage of Fig. 12 showing the lines of sight to B1849+005 and PSR B1849+00. The gray scale shows the smoothed, continuum-subtracted  $\text{H}\alpha$  emission on a linear scale from 0 to 10 Rayleighs. The sizes of the symbols are proportional to the scattering diameter (B1849+005) or upper limit (PSR B1849+00) at 1 GHz. For the scattering diameter of B1849+005, it is shown with the correct orientation and anisotropy.

the parameters  $n_e$  and  $F$  are highly correlated. The best-fit value for the distance to the clump is 4.7 kpc. While consistent with the crude estimate obtained above based on just the scattering diameters, this distance for the clump corresponds to  $x \approx 1/2$ . This value simply reflects the value of  $x$  that maximizes the modeled pulse broadening, which still only poorly reproduces the observed pulse broadening.

If the excess scattering toward both B1849+005 and PSR B1849+00 is attributed to the same clump, the angular diameters provide the most useful constraint: the clump must be at least 2.3 kpc distant. Given that no single clump reproduces all of the observations, it is quite likely that different clumps affect the two lines of sight.

Is there a structure along the line of sight that could contribute to anomalous scattering toward PSR B1849+00 but not B1849+005? Figure 13 shows the  $\text{H}\alpha$  emission in a small region around these two sources taken from the Southern H-Alpha Sky Survey Atlas (SHASSA; Gaustad et al. 2001). Clearly apparent between the two, but offset slightly toward PSR B1849+00, is a clump of slightly stronger  $\text{H}\alpha$  emission.

This  $\text{H}\alpha$  clump appears to lie on the outskirts of the H II region G33.418–0.004 (Lockman 1989). If this  $\text{H}\alpha$  clump is associated with the H II region, the  $\text{H}\alpha$  clump would represent only a small fraction of the total  $\text{H}\alpha$  luminosity of the H II region. Based on the recombination line strengths for the H II region, much of it must be heavily absorbed at optical wavelengths. This line of sight is toward the Aquila Rift (Dame et al. 2001), and the area to the south of the  $\text{H}\alpha$  clump appears consistent with being heavily obscured (Fig. 13).

The emission measure of this H II region is  $\text{EM} \approx 7000 \text{ pc cm}^{-6}$  (Lockman 1989). The  $\text{H}\alpha$  clump and the line of sight to PSR B1849+00 appear to be where the 5 GHz continuum has dropped by approximately a factor of 2 (Altenhoff et al. 1979). Thus, the EM contributed by the H II region along the line of sight to the pulsar is perhaps  $3500 \text{ pc cm}^{-6}$ . The equivalent scattering measure is  $\log \text{SM} = 0.81 [\text{kpc m}^{-20/3}]$ , assuming an outer scale of 1 pc (Cordes et al. 1991). This level of scattering is comparable to, though somewhat below,

that required for the line of sight to PSR B1849+00. The fitting procedure above produces a clump with  $\log SM = 1.4$ , but the scattering parameters of the clump in the Cordes-Lazio model imply  $\log SM = 3.6$ .

Although it seems reasonable to attribute some fraction of the scattering toward PSR B1849+00 to G33.418–0.004, the H II region does not appear to be capable of explaining it all. The line of sight to PSR B1849+00 would have to pierce several hundred similar H II regions. Higher-density filaments or tendrils from the H II region may be in front of the pulsar and responsible for the anomalous scattering, but the identification of such filaments must await H $\alpha$  observations of higher resolution and sensitivity.

Alternately, a larger SM would be obtained if the outer scale in G33.418–0.004 were  $l_0 \ll 10^{-4}$  pc ( $l_0 \ll 20$  AU). Given that the size of G33.418–0.004 is probably comparable to 1 pc, it is difficult to understand why the outer scale would be so much smaller. Moreover, the H II region is well offset from the location of B1849+005 (Altenhoff et al. 1979), so the enhanced scattering along the line of sight to the extragalactic source cannot be attributed to the H II region. As Spangler et al. (1986) concluded, the enhanced scattering toward B1849+005 (or PSR B1849+00) cannot be attributed to any single object or region.

## 5. CONCLUSIONS

I have observed the extragalactic source B1849+005 at frequencies between 0.33 and 15 GHz with the Very Large Array (VLA) and Very Long Baseline Array (VLBA) and reanalyzed archival VLA observations between 0.33 and 4.9 GHz. The source has a complex structure, as Fey et al. (1991) suggested, with components of emission both to the southwest and northeast of the central component. However, at least to 15 GHz, the central component is compact and highly scattered; our larger frequency range, nearly two orders of magnitude, extends the earlier analyses of Spangler et al. (1986) and Fey et al. (1991), who also found the source to be highly scattered.

I have analyzed the interferometric visibilities to extract parameters of the spectrum of density fluctuations responsible for scattering and compared the scattering of B1849+005 to other nearby sources. The density fluctuations are anisotropic, with an anisotropy of about 1.3, comparable to that seen for other highly scattered sources in the Galactic disk but less than that toward Galactic center sources. While the data are suggestive that the position angle of the anisotropy changes with frequency, the uncertainties are large. Nonetheless, it seems clear that density fluctuations are becoming anisotropic on scales of order  $10^{15}$  cm ( $D/5$  kpc). An inner scale to the density spectrum also appears necessary to reproduce the observed visibilities. The evidence for an inner scale  $l_1$  comes both from direct fits for a density spectrum including an inner scale as well as from assessing the values of the density spectral index  $\alpha$  for a power-law-only density spectrum. Both of these approaches suggest an inner scale of roughly a few hundred kilometers, comparable to that found toward other sources.

The two observations at 0.33 GHz span approximately a decade. There is essentially no change in the shape of the image over this interval. A conservative upper limit on the velocity of the scattering material is  $1800 \text{ km s}^{-1}$ . This value is sufficiently large that it does not exclude material from the supernova remnant G33.6+0.1 from contributing to the enhanced scattering along this line of sight.

In the 0.33 GHz image of the field around B1849+005, there is a number of other sources that might also be heavily scattered. As is seen in other regions of intense scattering (e.g., the Cygnus region and the Galactic center), there are large changes in the strength of scattering on lines of sight separated by a degree or less. With only a single frequency to estimate the scattering, not all of the large diameters in this region can be attributed to scattering. Nonetheless, many of the sources probably are heavily scattered, and these other sources in the field could serve as a useful starting point for future scattering observations in this direction.

Both B1849+005 and PSR B1849+00, which are separated by only  $13'$ , show extremely strong scattering, and PSR B1849+00 shows an anomalous frequency scaling for its pulse broadening between 1.4 and 2.7 GHz. While there is no indication of an anomalous frequency scaling for the angular broadening of B1849+005 above 5 GHz, the observations between 1.4 and 2.7 GHz (namely those at 1.5 and 2.3 GHz) are insufficient to place strong constraints on the presence of any anomalous frequency scaling. Moreover, the observations were insufficient for placing useful constraints on the angular broadening of PSR B1849+00; simultaneous observations of PSR B1849+00 and B1849+005 at 1.6 GHz are under way and will be reported elsewhere.

If the lines of sight to the pulsar and extragalactic source are affected by the same “clump” of scattering material, it must be at least 2.3 kpc distant. However, a detailed attempt to account for all of the scattering observables toward these sources (angular broadening of the extragalactic source, pulse broadening of the pulsar, and upper limits on the angular broadening of the pulsar) does not produce a self-consistent set of parameters for a clump that can reproduce all three measured scattering observables.

There is a clump of H $\alpha$  emission that lies in between the lines of sight to PSR B1849+00 and B1849+005, which is associated with an unobscured part of the H II region G33.418–0.004. However, unless conditions within this H II region are unusual, it appears unable to produce a sufficient amount of scattering to explain the excess scattering along both (or even either) lines of sight. As Spangler et al. (1986) concluded, the scattering toward either B1849+005 or PSR B1849+00 cannot be attributed to a single object or region.

I thank R. Mutel for the initial encouragement to undertake this project, S. Spangler for helpful discussions regarding scattering and structure functions and for providing his fitting routines, A. Fey for discussions about the structure of B1849+005, the referee for a number of comments that improved the presentation of this work, and D. Boboltz, A. Fey, and R. Gaume for their hospitality at the US Naval Observatory, where much of the analysis was performed. I thank the individuals involved in the Southern H-Alpha Sky Survey Atlas (SHASSA), which is supported by the National Science Foundation, for making their results easily available. This research has made use of NASA’s Astrophysics Data System bibliographic services and of the SIMBAD database, operated at CDS, Strasbourg, France. The VLA and the VLBA are facilities of the National Science Foundation operated under cooperative agreement by Associated Universities, Inc. A portion of this work was conducted while the author was a National Research Council Research Associate at the Naval Research Laboratory (NRL). Basic research in radio astronomy at the NRL is supported by the Office of Naval Research.

## REFERENCES

- Alberdi, A., et al. 1993, *A&A*, 277, L1
- Altenhoff, W. J., Downes, D., Pauls, T., & Schraml, J. 1979, *A&AS*, 35, 23
- Armstrong, J. W., Rickett, B. J., & Spangler, S. R. 1995, *ApJ*, 443, 209
- Briggs, D. S., Schwab, F. R., & Sramek, R. A. 1999, in *ASP Conf. Ser.* 180, *Synthesis Imaging in Radio Astronomy II*, ed. G. B. Taylor, C. L. Carilli, & R. A. Perley (ASP: San Francisco), 127
- Chandran, B. D. G., & Backer, D. C. 2002, *ApJ*, 576, 176
- Clegg, A. W., Fiedler, R. L., & Cordes, J. M. 1993, *ApJ*, 409, 691
- Clifton, T. R., Frail, D. A., Kulkarni, S. R., & Weisberg, J. M. 1988, *ApJ*, 333, 332
- Coles, W. A., Rickett, B. J., Codona, J. L., & Frehlich, R. G. 1987, *ApJ*, 315, 666
- Condon, J. J., Cotton, W. D., Greisen, E. W., Yin, Q. F., Perley, R. A., Taylor, G. B., & Broderick, J. J. 1998, *AJ*, 115, 1693
- Cordes, J. M., & Lazio, T. J. 1991, *ApJ*, 376, 123
- . 2001, *ApJ*, 549, 997
- . 2003, *ApJ*, submitted
- Cordes, J. M., Weisberg, J. M., Frail, D. A., Spangler, S. R., & Ryan, M. 1991, *Nature*, 354, 121
- Cornwell, T. J., & Perley, R. A. 1992, *A&A*, 261, 353
- Dame, T. M., Hartmann, D., & Thaddeus, P. 2001, *ApJ*, 547, 792
- Dennison, B., Broderick, J. J., Thomas, M., Booth, R. S., Brown, R. L., & Condon, J. J. 1984, *A&A*, 135, 199
- Desai, K. M., & Fey, A. L. 2001, *ApJS*, 133, 395
- Desai, K. M., Gwinn, C. R., & Diamond, P. J. 1994, *Nature*, 372, 754
- Dickey, J. M., Kulkarni, S. R., Heiles, C. E., & van Gorkom, J. H. 1983, *ApJS*, 53, 591
- Fey, A. L., Spangler, S. R., & Cordes, J. M. 1991, *ApJ*, 372, 132
- Fey, A. L., Spangler, S. R., & Mutel, R. L. 1989, *ApJ*, 337, 730
- Frail, D. A., Diamond, P. J., Cordes, J. M., & van Langevelde, H. J. 1994, *ApJ*, 427, L43
- Frail, D. A., & Weisberg, J. M. 1990, *AJ*, 100, 743
- Furst, E., Reich, W., Reich, P., & Reif, K. 1990, *A&AS*, 85, 805
- Gaustad, J. E., McCullough, P. R., Rosing, W., & Van Buren, D. 2001, *PASP*, 113, 1326
- Gupta, Y., Rickett, B. J., & Lyne, A. 1988, in *AIP Conf. Proc.* 174, *Radio Wave Scattering in the Interstellar Medium*, ed. J. M. Cordes, B. J. Rickett, & D. C. Backer (New York: AIP), 140
- Hewish, A., Wolszczan, A., & Graham, D. A. 1985, *MNRAS*, 213, 167
- Jauncey, D. L., et al. 1989, *AJ*, 98, 44
- Lambert, H. C., & Rickett, B. J. 1999, *ApJ*, 517, 299
- Lazio, T. J. W. 1997, Ph.D. thesis, Cornell Univ.
- Lazio, T. J. W., & Cordes, J. M. 1998, *ApJ*, 505, 715
- Lazio, T. J. W., Spangler, S. R., & Cordes, J. M. 1990, *ApJ*, 363, 515
- Lithwick, Y., & Goldreich, P. 2001, *ApJ*, 562, 279
- . 2003, *ApJ*, 582, 1220
- Lo, K. Y., Backer, D. C., Ekers, R. D., Kellermann, K. I., Reid, M., & Moran, J. M. 1985, *Nature*, 315, 124
- Lockman, F. J. 1989, *ApJS*, 71, 469
- Löhmer, O., Kramer, M., Mitra, D., Lorimer, D. R., & Lyne, A. G. 2001, *ApJ*, 562, L157
- Marcaide, J. M., Alberdi, A., Lara, L., Perez-Torres, M. A., & Diamond, P. J. 1999, *A&A*, 343, 801
- Molnar, L. A., Mutel, R. L., Reid, M. J., & Johnston, K. J. 1995, *ApJ*, 438, 708
- Moran, J. M., Greene, B., Rodríguez, L. F., & Backer, D. C. 1990, *ApJ*, 348, 147
- Narayan, R. 1992, *Philos. Trans. R. Soc. London*, 341, 151
- Perley, R. A. 1989, in *ASP Conf. Ser.* 6, *Synthesis Imaging in Radio Astronomy*, ed. R. A. Perley, F. R. Schwab, & A. H. Bridle (San Francisco: ASP), 287
- Ramachandran, R., Mitra, D., Deshpande, A. A., McConnell, D. M., & Ables, J. G. 1997, *MNRAS*, 290, 260
- Reid, M. J., Readhead, A. C. S., Vermeulen, R. C., & Treuhaft, R. N. 1999, *ApJ*, 524, 816
- Rickett, B. J. 1990, *ARA&A*, 28, 561
- Romani, R. W., Narayan, R., & Blandford, R. 1986, *MNRAS*, 220, 19
- Slysh, V. I., et al. 2001, *MNRAS*, 320, 217
- Spangler, S. R., & Cordes, J. M. 1988, in *AIP Conf. Proc.* 174, *Radio Wave Scattering in the Interstellar Medium*, ed. J. M. Cordes, B. J. Rickett, & D. C. Backer (New York: AIP), 117
- . 1998, *ApJ*, 505, 766
- Spangler, S. R., & Gwinn, C. R. 1990, *ApJ*, 353, L29
- Spangler, S. R., Mutel, R. L., Benson, J., & Cordes, J. M. 1986, *ApJ*, 301, 312
- Stanimirovic, S., Weisberg, J. M., Dickey, J. M., de la Fuente, A., Devine, K., Hedden, A., & Anderson, S. B. 2003, *ApJ*, 592, 953
- Taylor, J. H., & Cordes, J. M. 1993, *ApJ*, 411, 674
- Trotter, A., Moran, J., & Rodríguez, L. 1998, *ApJ*, 493, 666
- van Gorkom, J. H., Goss, W. M., Seaquist, E. R., & Gilmore, W. S. 1982, *MNRAS*, 198, 757
- van Langevelde, H. J., Frail, D. A., Cordes, J. M., & Diamond, P. J. 1992, *ApJ*, 396, 686
- Wilkinson, P. N., Narayan, R., & Spencer, R. E. 1994, *MNRAS*, 269, 67
- Wolszczan, A., & Cordes, J. M. 1987, *ApJ*, 320, L35
- Yusef-Zadeh, F., Cotton, W., Wardle, M., Melia, F., & Roberts, D. A. 1994, *ApJ*, 434, L63